ARC WELDING OF DISSIMILAR STAINLESS STEEL FILLET WELDS

MATUS GELATKO[1], RADOSLAV VANDZURA[1], BRANISLAV VASKOVIC[1], FRANTISEK BOTKO[1], MICHAL HATALA[1], SVETLANA RADCHENKO[1]

[1]Technical University of Kosice, Faculty of Manufacturing Technologies with a seat in Presov, Slovakia

DOI: 10.17973/MMSJ.2025_10_2025080

matus.gelatko@tuke.sk

The fusion welding of additively manufactured (AM) materials in the important issue for their reliable application within the structures, which demands the conduction of related research. The paper is focused on a testing of Metal Active Gas (MAG) welding of conventionally manufactured (CM) and AM stainless steel 316L (Selective Laser Melting - SLM). The main objective is the examination of the weldability of AM stainless steel in various combinations with its CM equivalent within fillet welds. The selected filler metal, gas mixture and welding parameters are evaluated through the macrostructure and microstructure analysis of the parent metals (PM), weld metal (WM) and heat affected zone (HAZ). Obtained results represent important preliminary data for the next direction of wider research focused on fusion welding research of SLM stainless steel, and they serve as the base for the assumptions of welding parameters optimization with the outline of future research activities.

KEYWORDS

fusion welding, MAG welding, GMAW welding, additive manufacturing, selective laser melting, 316L

1 INTRODUCTION

During the rapid advancement of modern technologies in recent years, components created using the additive manufacturing (AM) technologies found its stable place within their applications as the real industrial components of functional assemblies. However, the related research activities are still necessary for the increasing of final quality. The important issue is their reliable incorporation into the mentioned assemblies, mainly in the case of AM metal components, where the application of fusion welding methods is inseparable part of this process [Gill 2020].

In laboratory conditions, the successful solutions included more specific methods, predominantly based on the physical principles using the high energy beam, which are also naturally used for the Powder Bed Fusion processes [Patterson 2021]. The laser beam welding showed the possibility of reaching the reliable joints of AM Ti6Al4V titanium alloy, which in comparison with joint of its wrought equivalent reached wider bead width, higher microhardness and vice versa, lower tensile strength and ductility [Omoniyi 2022]. Caiazzo, F. and Alfieri, V. [Caiazzo 2021] provided the optimization of stainless steel laser beam welding in the form of the monitoring of laser power, its speed and defocusing with the subsequent evaluation of experiment, considering the international standards for welding. AlSi10Mg aluminium alloy welds exhibit not negligible amount of porosity, also at using the more sophisticated welding methods, such as electron beam welding (EBW). A certain solution was proposed for the EBW joints composed of conventionally made (CM) and AM AlSi10Mg, in the form of three-spot welding technique in a combination with adjusted parameters, which cannot be the same with the parameters for conventional type. However, the porosity was transferred from the weld metal to the fusion line on the AM side [Michler 2021]. Dissimilar (hybrid) welds were similarly created using the EBW, but the material of interest was Inconel 718 alloy [Sali 2022]. The evaluation of experimental specimens showed that the welded L-PBF material reached higher yield strength and tensile strength, nevertheless, a ductility was better in the case of conventional one. Resulting suggestions include using the best possible AM parameters for the full melting of powder, the application of post-processing operations and using of the electron beam oscillation during the EBW.

In the industrial practice, more frequently utilized are welding methods, working on the principle of electric arc. A Tungsten Inert Gas (TIG) welding method showed good potential for welding the AM products within recent studies, where created joints were compared with laser beam welded joints including aluminium alloy AlSi10Mg [Zhang 2019], or titanium alloy Ti6Al4V [Sen 2023]. A complex study [Faes 2024] showed that it is possible to sufficiently weld the AM 316L stainless steel (including dissimilar joints with conventional equivalent) with compared welding methods: laser beam, manual TIG, manual MIG/MAG and robotic MIG/MAG. The primary experiment conducted by Huysmans, et al. [Huysmans 2021] showed that it is possible to weld the AM 316L stainless steel using the TIG method, which was verified by the mechanical and corrosion tests on welded pipes (AM/CM). The application of method was also confirmed for the welding of SLM AISI 316L stainless steel, whereas the application of appropriate filler metal and heat treatment can increase the quality of joints [Mohyla 2022]. The study [Kuehn 2024] focused on the evaluation of tensile behaviour, grain size, microhardness and secondary dendrite arm spacing within dissimilar stainless steel welds, pointed on the fact that the AM 316L had better weldability than the used conventional equivalent. The mechanical behaviour of 316L dissimilar butt welds (created using the Gas Metal Arc Welding - GMAW method) can be influenced by the microstructure, presence of smaller defects, and residual stresses which are also affected by the building direction of AM parent metals and their orientation within the joint [Mascenik 2020, Braun 2023]. During the tensile and fatigue testing of Pulsed GMAW joints, AM 316L material reached the similar results as its CM equivalent [Saga 2020, Selmi 2023].

Despite the fact that high energy beam welding technologies can reliably fuse AM components, the application of arc method is more suitable for the industrial practice. Considering the requirements for reaching of the sufficient quality joints, the selection of appropriate filler material, shielding gas and setting of welding parameters are significant factors, which influence the weldability of a material, especially in the case of more specific materials, such as stainless steels. The more demanding is welding of AM materials, where 100% density of parent material is restricted. The lack of studies, focused on the experiments of MIG/MAG/GMAW welding of AM components straightly set the motivation of this research. The described experiment describes preliminary testing of MAG welding applied on the CM and AM stainless steel 316L, with the objective of the macrostructure and microstructure evaluation of CM-CM, CM-AM, AM-CM, AM-AM fillet welds, according to selected welding parameters. Obtained results are important input data for the optimization of welding parameters a design of the main experiment, focused on the evaluation of mechanical properties and other related characteristics of such dissimilar joints.

2 MATERIALS AND METHODS

The base of experimental materials was austenitic stainless steel. The first selected was conventional type AISI 316L and the second was its additive manufactured equivalent with label SS 316L. The composition and main the properties are included in following Tab. 1, Tab. 2, and Tab. 3.

Table 1. Chemical composition of AISI 316L stainless steel [Matweb 2025]

Element	Mass (%)	Element	Mass (%)
Fe	Balance	**Si**	≤ 1
Cr	16 - 18	**P**	≤ 0.045
Ni	10 - 14	**C**	≤ 0.03
Mo	2 - 3	**S**	≤ 0.03
Mn	≤ 2		

Table 2. Chemical composition of SS 316L stainless steel [Renishaw 2025]

Element	Mass (%)	Element	Mass (%)
Fe	Balance	**N**	≤ 0.1
Cr	16 - 18	**O**	≤ 0.1
Ni	10 - 14	**P**	≤ 0.045
Mo	2 - 3	**C**	≤ 0.03
Mn	≤ 2	**S**	≤ 0.03
Si	≤ 1		

Table 3. Mechanical and physical properties of materials [Matweb 2025, Renishaw 2025]

Parameter	Direction	AISI 316	SS 316L (As built)
Density [g·cm^{-3}]	-	8.00	7.99
Hardness [HV]	XY	152	198 ± 8 *
	Z		208 ± 6 *
Yield strength [MPa]	XY	235	547 ± 3
	Z		494 ± 14
Elongation at break [%]	XY	55	43 ± 2
	Z		35 ± 8
Modulus of elasticity [GPa]	XY	193	197 ± 4
	Z		190 ± 10
Thermal conductivity [W·mK^{-1}]	-	14 - 15.9	16.2
Melting point [°C]	-	1375 – 1400	1371 – 1399

* Vickers hardness HV0.5

The additive manufactured specimens were made using the Selective Laser Method (SLM), during which the material in the form of powder is melted and transformed into the solid state by the influence of a laser beam. The final component is made layer-by-layer based on the designed shape. Specimens were prepared in the Technical University in Ostrava (Czech Republic) – Center of 3D printing Protolab, using the RenAM500S Flex machine. The system includes chamber with dimensions 250 x 250 x 350 mm, in which the components can be printed at production speed of 5-20 cm3.h-1, using a laser power up to 500 W, a scanning speed up to 2000 mm.s-1, a positioning speed up to 7000 mm.s-1 and a layer thickness in the range of 20 and 100 µm. The parameters selected for the creation of experimental specimens are included in the following table.

Table 4. SLM parameters

Parameter	Value
Laser power P [W]	200
Scanning velocity v [mm·s^{-1}]	650
Hatch distance d [µm]	110
Layer thickness t_L [µm]	50
Energy input ε [J·mm^{-3}] (1) [Gu 2009] **Chyba! Nenalezen zdroj odkazů.**	55.94
Scanning strategy (Fig. 1)	Chessboard
Gas protection	Argon (Ar)

$$\varepsilon = \frac{P}{v \cdot d \cdot t_L} \quad (1)$$

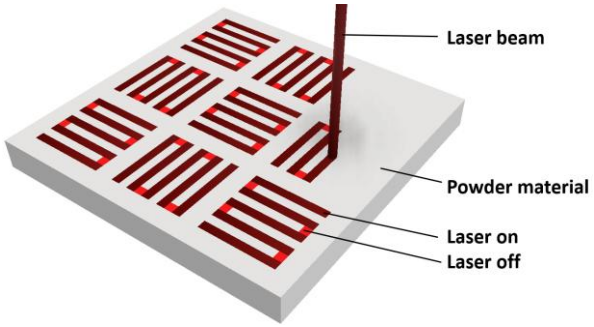

Figure 1. Chessboard scanning strategy [Renishaw 2025]

Dimensions of parent metals for the final experimental fillet welds were same for both, conventional and additive manufactured materials (50 x 30 x 5 mm). The width of a conventional specimens for the bottom part was 50 mm. The experimental welding was conducted in the Faculty of Manufacturing Technologies (Technical University of Kosice) using the MAG method with the Lorch S3 mobil Pulse XT machine, which is air-cooled, in dimensions of 812 x 340 x 518 mm. The range of welding current is 250–320 A for both, MIG or MAG method, a machine provides possibilities in a selection of specific welding regimes and application of SMAW method. As the shielding gas, Inoxline H2 by the Messer Tatragas company was used. The gas is composed of 98% Argon (Ar) and 2% Carbon Dioxide (CO2), whereas this mixture is primarily intended for the welding of stainless steels. The used wire was Thermanit GE-316L Si by Bohler Welding company with the 1 mm diameter. The chemical composition and mechanical properties are included in Tab. 5 and Tab. 6.

Table 5. Chemical composition of Thermanit GE-316L Si wire [Bohler Welding 2014]

Element	Mass (%)	Element	Mass (%)
C	0.02	**Cr**	18.8
Si	0.8	**Mo**	2.8
Mn	1.7	**Ni**	12.5

Table 6. Mechanical properties of Thermanit GE-316L Si wire [Bohler Welding 2014]

Parameter	Value
Yield strength $R_{p0.2}$ [MPa]	380
Yield strength $R_{p1.0}$ [MPa]	420
Tensile strength [MPa]	560
Elongation (L_0=5d_0) [%]	35

Impact work ISO-V KV J [+20 °C]	70

For the identification of surface reaching defects on welds, non-destructive penetrant testing method was applied. The complex set of Nord-Test (Helling company) cleaner, penetrant and developer were used. After the cleaning process, dwell time of penetration was for 10 minutes with following removing of penetrant, application of developer and investigation of indications after 10 and 30 minutes. A digital microscope Keyence VHX-7000 was used for the evaluation of macroscopic and microscopic characteristics.

2.1 Setting of welding parameters

In the first stage of the experiment, welding parameters were adjusted on the conventional AISI 316L fillet welds composed of 5 mm thick plates. Concretely, voltage (U) and wire feed rate (f) were adjusted and the welding current (I) alongside with weld characteristics were monitored. The first set of combinations (Tab. 7) included various values of voltage and fire feed, whereas the primary objective was to evaluate the variation of U parameter.

Table 7. Combinations of welding parameters during adjustment (U, f)

Combination	U [V]	f [m·min^{-1}]	I [A]
1	16.5	4	96
2	17.5	5	104
3	18.5	6	123
4	19.5	7	145
5	20.5	8	157

The following Fig. 2 includes interpretation of welds created at combination 1, 3 and 5. It can be seen that in the case of lower welding parameters, the weld is excessive (convexity) in the middle and its toes exhibit sharp transition into the parent metal, which increase the probability of creation the grooves, which are the natural sources for the creation of cracks. Vice versa, the weld created at higher welding parameters is characterised by larger crater and probable effect of higher induced heat caused the burnout and excessive melting of parent metals. The optimal fillet weld tent to be reached at using the 18.5 V, where smooth transition of weld into the parent metal, without the evident convexity and with the typical weld texture. Also, the welding current value at this combination is on the favourable value (123 A). Previously mentioned influence of induced heat can be seen on the opposite side and the bottom side of the welds. The increasing area of heat affected zone is dependent on the increasing of welding parameters, whereas the very high influence can cause significant deformations and very low influence can cause insufficient creation of joint.

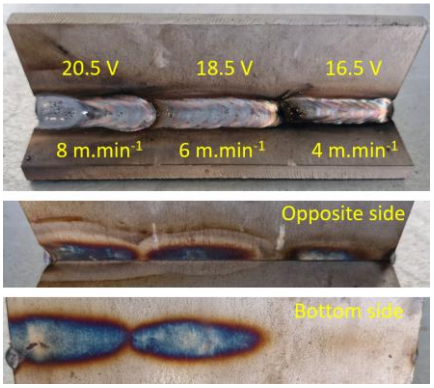

Figure 2. Welds of combinations 1, 3 and 5 from Tab. 7

The following within the adjusting of welding parameters was the evaluation of the wire feed rate (f) influence at the selected value of voltage (U). The following Tab. 8 includes five combinations of variable wire feed rate (f) at the contestant voltage (U) on the 18.5 V.

Table 8. Combinations of welding parameters during adjustment (f)

Combination	f [m·min^{-1}]	I [A]
1	5	112
2	5,5	119
3	6	124
4	6,5	131
5	7	146

The following Fig. 3 includes the interpretation of three welds at 5, 6 and 7 m.min^{-1}. The welds are more similar to each other than in the case of variable voltage (Fig. 2), whereas the smooth transition into the parent metal is present in all three welds. The weld created at the lowest wire feed rate has less consistent texture of face, the filler metal is rapidly melted, and the weld pool do not penetrate deeper into the material. The texture of a weld created at the middle value of wire feed rate is more consistent, hence, better penetration of a weld pool can be expected. Using the highest value of weld in a selected range, parent metals are more influenced, a crater is more noticeable and in overall, weld seem to be larger what can cause the scenario where materials can be significantly influenced by the heat. The area influenced by the induced heat can be seen from the opposite and bottom side, whereas its size increases with the increase of wire feed rate. The influenced area of 6 and 7 m.min-1 is similar with the indication of a little higher heat presence at the highest wire feed rate, and the not negligibly low influence at the lowest value of wire feed rate (5 m.min-1) can be the sign that the fusion of parent metals is insufficient.

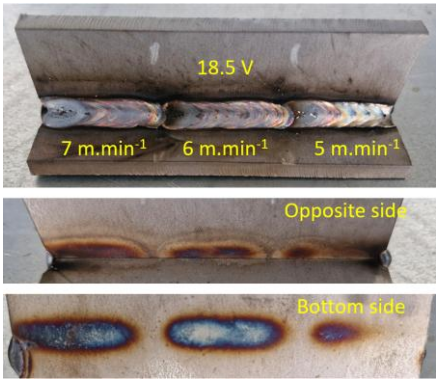

Figure 3. Welds of combinations 1, 3 and 5 from Tab. 8

3 RESULTS

Four experimental specimens were prepared for the final evaluation of welding the conventionally manufactured (CM) and additively manufactured (AM) stainless steel. Parent metals were 5 mm thick and 50 mm long. The width of vertical sheets was 30 mm, and for the horizontal sheets, a width was 50 mm for CM material and 30 mm for AM material. The combinations of parent metals for experimental specimens are included in the Fig. 4. The sheets were situated at 90° angle and welded with spots on both sides. Based on the debugging of parameters, experimental specimens were welded at parameters included in Table 9.

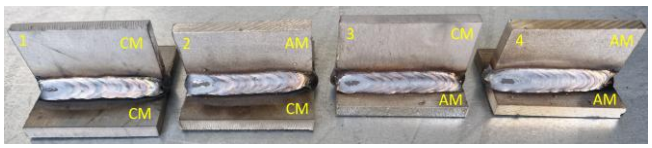

Figure 4. Experimental specimens

Table 9. Experimental welding parameters

Number of specimens	4
Type of weld	Fillet
Number of passes	1
Wire diameter	1 mm
Gas flow	15 $l.min^{-1}$
Voltage (U)	18.5 V
Wire feed rate (f)	6.5 $m.min^{-1}$
Welding current (I)	131 A

3.1 Penetrant testing

The following Fig. 5 depicts the result of the penetrant testing on experimental welds during the examination of indications after 30 minutes. The presence of transverse indications (arrows) was observed on ends of the welds 1, 2 and 3 with dimension in the range of 1 and 2 mm. These indications are referred to the pits, probably caused by the immediate motion of torch after the ignition of the electric arc, and vice versa, its rapid interruption and removing the torch (wire) out of the welding area, which is present on the end of a weld 1. Considering the small size of these defects and the fact that the area of interest was the middle part of the specimens, their significance can be neglected. Areas highlighted with ellipses points on the presence of spatters which are common during the welding process, especially in the case of welding the stainless steel. Taking this fact and the small amount of them into account, their influence within this research is irrelevant.

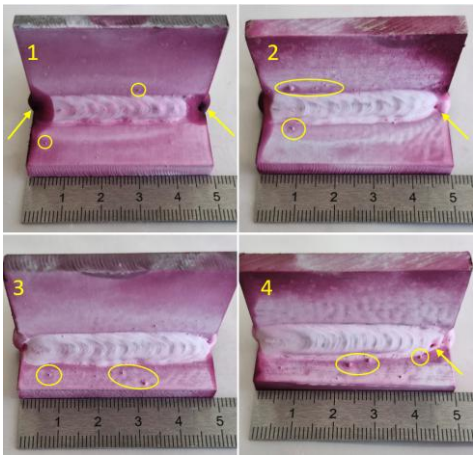

Figure 5. Penetrant testing of experimental specimens

3.2 Macroscopic analysis

Macroscopic and microscopic characteristics of 4 experimental welds were done on metallographic specimens cut from the middle. They were prepared using the grinding papers of grit P120, P320, P1200, P2500 and P4000, polished using the cloth and abrasive particles (3 µm), with subsequent etching for 10 second using the Nital (5% solution). The specimen 1 is composed of two parent metals made from conventional stainless steel (Fig. 6). The gap between the sheets is minimal, which indicates their appropriate positioning during the preparation of specimens. A created fillet weld has slightly excessive face (convexity), however toes are connected to parent metals without grooves, which suppresses the probability of cracks´ occurrence and propagation. A more significant penetration of weld (fusion zone) is present on the side of a vertical sheet, what is the consequence of torch angle during the welding in this area. The cavity in the corner of weld indicates low root penetration, hence, it would be appropriate to use higher welding parameters or decrease the welding speed. The heat affected zone (HAZ) is very slightly visible on the bottom horizontal sheet.

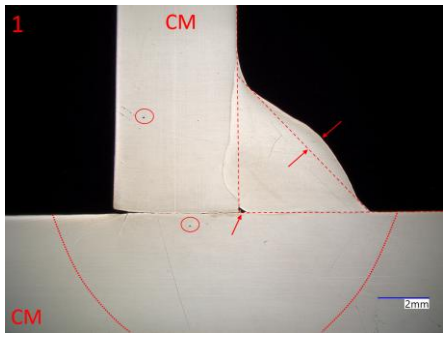

Figure 6. Macroscopic view of specimen 1

The following Fig. 7 includes macroscopic view on specimen 2, which includes parent metals of CM stainless steel (horizontal sheet) and AM stainless steel (vertical sheet). The gap between parent metals is minimal on the side of the weld and slightly wider on the opposite side, reaching approximately to the half of the vertical sheet. The reason of its occurrence can be the irregular shape of the AM sheet or its bending in the direction of the weld seam under the influence of heat during the welding. The convexity of face is more significant than in the case of specimen 1, similarly with the smooth transition of toes into the parent metals. The fusion zone is sufficient and equivalent in both parent metals. Also, during the welding of specimen 2, a weld pool was unable to penetrate the corner of sheets, hence the lack of root penetration occurred. The HAZ is more evident on the left side of the horizontal CM parent metal. The small amount of porosity was observed in both parent metals and 2 negligible pores are present in the weld metal, probably transformed from parent metals during the welding.

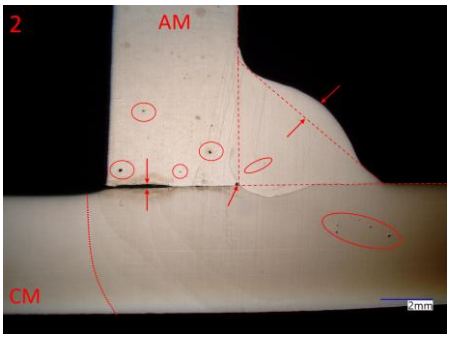

Figure 7. Macroscopic view of specimen 2

The specimen 3 (Fig. 8) is similarly composed of one CM and one AM parent metal but with the reverse positions than within the specimen 2. The gap between parent metals is minimal with the slight opening on the opposite side of the weld, caused by the bending phenomenon under the influence of heat. Convexity with smooth transition into the parent metals again occurred in this case.

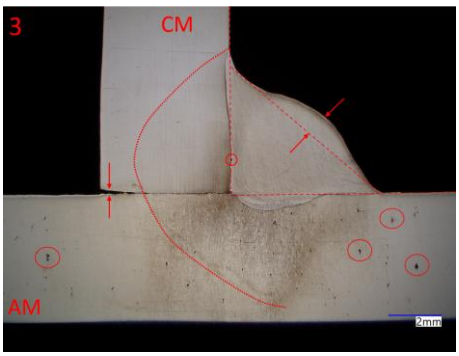

Figure 8. Macroscopic view of specimen 3

The variation of a torch angle caused the larger area of fusion zone in the AM parent metal. For this specimen, selected parameters were sufficient, and lack of root penetration did not occur. It is possible to assume that the welding speed was also appropriate. The HAZ is visible on both parent metals, approximately up to the depth of 2/3 thickness of sheets. A porosity in the form of randomly distributed cavities was observed mainly in the AM stainless steel, what can be the most likely caused by the SLM technology. A single cavity is present on the fusion line of CM parent metal, whereas it was supposedly transformed from the parent metal.

The shape characteristics of weld on specimen 4 (two AM parent metals) are analogical (Fig. 9). Minimal gap with thin variabilities caused by the uniform surface geometry of SLM sheets, slight convexity and smooth transition of toes into the parent metals. The fusion zone is more significant on the vertical sheet with the slight lack of root penetration. The HAZ is mainly visible on the horizontal sheet. Both parent metals include cavities in the form of larger single cavities and porosity clusters. However, they were not transformed into the weld metal significantly.

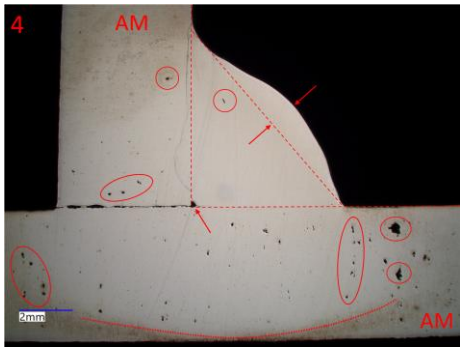

Figure 9. Macroscopic view of specimen 4

3.3 Microscopic analysis

The following Fig. 10 compares microstructure of CM AISI 316L and AM SS 316L parent metals within the specimen 3. The characteristics of CM microstructure are standardly polyhedral for this kind of stainless steel. Included grains reach dimension in the range of 10 up to 100 µm in the equiaxed shape with the irregular shape. Furthermore, the microstructure includes typical annealing twins and the presence of heterogenous precipitates of carbide phases from alloying elements (mainly Cr and Ni), irregularly dispersed within the matrix. Commonly occurring defects in the form of cavities or inclusions arising during the metallurgical process were not observed in the evaluated area of this parent metal. The AM SS 316L material is characterized by the spherical grains, creating the substructure defined by the melt pools solidified layer-by-layer during the SLM process in a layering direction. The specific circumstances of SLM process influence, as the size of grains, so the substructure characteristics. The size is primarily defined by the penetration abilities of individual melt pools, the bonding of individual layers and interactions of mentioned melt pools on the level of one layer and interlayer. Hence, the grain size is different in the parallel and perpendicular direction to the layering, whereas it is approx. 100 µm and 30 – 50 µm, respectively. The grains are composed of dendritic structure with a tendency of orientation in the direction of solidification during the cooling of individual melt pools. The grain boundaries are more noticeable, which is the consequence of rapid recrystallization caused by the faster solidification, leading to the presence of segregation. The presence of precipitates with the nature of carbide phases of alloying elements is not so unambiguous as in the matrix of CM parent metal. Similarly, any discontinuities were not observed in the AM parent metal.

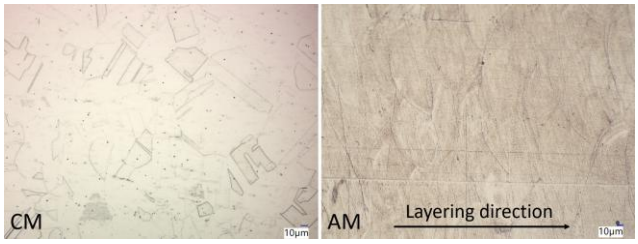

Figure 10. Microstructure of 316L parent metals

Due to the use of identical parameters during the experimental welding, the same microstructure of weld metal was reached in all 4 experimental specimens (Fig. 11), and the different manufacturing technology of parent metals did not influence its characteristics. The weld pool solidified into the dendritic microstructure, which arising is conditioned by the rapid heat removal during the cooling process after the heat impact of electric arc when the nuclei of solid solution in the liquid metal are not able to form into the typical polygonal shape. In overall, the epitaxial growth of grains caused the texture oriented in a diagonal direction, what is the consequence of solidification of weld pool in a direction between a root and a face of the fillet weld. With the focus on defects at the microstructure level, any cracks, cavities or inclusions were observed in the examined weld metal.

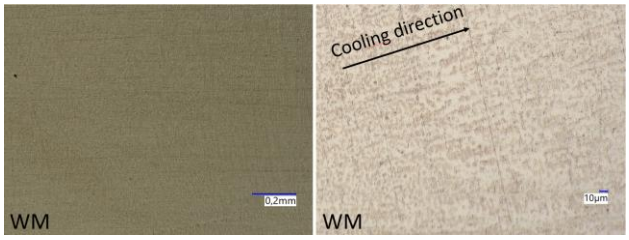

Figure 11. Microstructure of weld metal

The heat-affected zone (Fig. 12) of both parent metals, conventionally and additively manufactured, is without the distinctive variation of the microstructure, hence the recrystallization of austenitic matrix was not present to a significant extent. The transition of the weld metal into the parent metals is fluent and the microstructure changes right on the boundary, with the sufficient joint including the fusion line with segregations. On a detail of the fusion line of AM - WM metals can be seen that the HAZ of AM material includes characteristic spherical shaped grains, hence the morphological transformation did not occur in this area. On the side of the weld metal, a distinctive transition zone was observed in the area of root, mainly on the side of the AM parent metal. This zone includes columnar crystals oriented in a cooling direction of weld pool, which arises during the mixing of weld pool and influenced parent metal. The rapid solidification also contributes to the creation of such grains, when there is restricted time for the full recrystallization of a material.

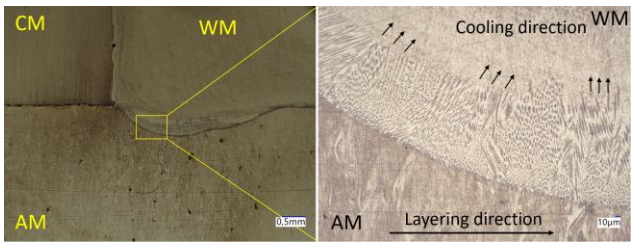

Figure 12. Microstructure of heat-affected zone

4 DISCUSSION

The comparison of obtained resulting data with the findings in studies from the field is the necessary part for the next optimization and regarding the subsequent direction of research. The weldability of SLM 316L stainless steel, including the creation similar and dissimilar joints using the MAG welding, was clearly confirmed with other studies [Braun 2023, Faes 2024, Selmi 2023]. Considering that mentioned studies were dedicated to the creation of butt welds, the approach of this experiment within the creation of fillet welds represents a certain added value. The application of 316L Si wire (similar to study [Braun 2023]) and gas mixture 98% Ar with 2% CO_2 (similar to study [Selmi 2023]) confirmed their suitability for the welding of 316L stainless steel (CM and AM). The voltage (U) for welding within mentioned studies was 21.5 V and 20 V for butt welds, respectively. Considering that fillet welds were created within this experiment, used voltage and adjusted wire feed rate are similar. Observed microstructure is identical with related studies focused on the arc welding, in the form of equiaxed grains and annealing twins of CM 316L stainless steel [Braun 2023, Faes 2024] and spherical grains defined by melt pools (perpendicular to the layering direction) of AM 316L stainless steel [Huysmans 2021, Mohyla 2022]. It also applies to the observation of dendritic microstructure in the weld metal [Faes 2024, Kuehn 2024, Mohyla 2022] and the HAZ, which microstructure is identical with the parent metals [Selmi 2023]. The presence of spatters was observed on both PMs (as the consequence of MAG welding characteristics – similar to [Selmi 2023]) and the porosity was observed mainly in the AM 316L BM, conditioned by the characteristics of its manufacturing process (similar to [Huysmans 2021, Selmi 2023]), but the possibility of its transformation into the WM is significantly lower than in the case of AM aluminium alloy [Zhang 2019].

5 CONCLUSIONS

The conducted experiment is focused on the preliminary testing of the MAG welding method application for the creation of AM and CM 316L stainless steel fillet welds, whereas the weldability and used welding parameters suitability are expressed using the macroscopic and microscopic analysis. Based on obtained resulting data, following conclusions are the most important:

- AM (SLM 316L) stainless steel exhibited satisfactory weldability within fillet welds of AM and CM equivalents, whereas selected Thermanit GE-316L Si wire with a shielding gas Inoxline H2 is the appropriate combination of a welding setup.
- The fusion of parent metals was reached, but it would be more suitable to select higher welding voltage, wire feed rate, welding speed and stable tilt angle for the securing of more sufficient weld pool penetration.
- Macroscopic analysis of four experimental welds showed slight excessive face (convexity), smooth transition of toes into the parent materials and local lack of root penetration.
- Microscopic analysis showed austenitic character for both parent metals. The polyhedral equiaxed grains were present within CM stainless steel and spherical grains within AM stainless steel, defined by the SLM melt pools. WM microstructure is dendritic with columnar crystals observed near the fusion line, whereas the HAZ is characterized by the fluent transition between WM and PM with the microstructure identical to the PM.
- Penetrant testing revealed any significant indications in the evaluated area of welds, but a certain porosity was observed in the AM parent metal, with a negligible transition into the weld metal. Small number of spatters indicates appropriate gas flow.

Even though the results point on some insufficiencies of evaluated experimental welds, a data is very important for the design of subsequent experiments or optimizations, and also for setting the appropriate parameters of AM stainless steel welds. Subsequent experiments need to be focused on the optimization of welding parameters and evaluation of mechanical properties and residual stresses. The results also outlined the consideration of the possibility in using the torch fixture with a drive and testing specific regimes of the used welding machine for the quality increasing of joints.

ACKNOWLEDGMENTS

This work was funded by the Slovak Research and Development Agency under contracts No. APVV-21-0228 and No. VV-MVP-0190. The projects VEGA 1/0391/22 and KEGA 017TUKE-4/2023 were granted by the Ministry of Education, Science, Research and Sport of the Slovak Republic. This article is the result of the following project implementation: Development of excellent research capacities in the field of additive technologies for the Industry of the 21st century, ITMS: 313011BWN5, supported by the Operational Program Integrated Infrastructure funded by the ERDF.

REFERENCES

[Bohler Welding 2014] Bohler Welding. Thermanit GE-316L Si [online]. 2014. Available from www.alruqee.com/Userfiles/Product/TablePdf/13042016000000T_Thermanit%20GE-316L%20Si_sow.pdf.

[Braun 2023] Braun, M., et al. Mechanical behavior of additively and conventionally manufactured 316L stainless steel plates joined by gas metal arc welding. Journal of materials research and technology, 2023, Vol. 24, pp. 1692-1705.

[Caiazzo 2021] Caiazzo, F., Alfieri, V. Optimization of laser beam welding of steel parts made by additive manufacturing. The International Journal of Advanced Manufacturing Technology, 2021, Vol. 114, No. 9, pp. 3123-3136.

[Faes 2024] Faes, K., et al. Weldability of additively manufactured powder bed fusion 316L stainless steel using arc and laser welding. Crystals, 2024, Vol. 14, No. 4, 303.

[Gill 2020] Gill, M., et al. Joining technologies for metal additive manufacturing in the energy industry. Jom, 2020, Vol. 72, No. 12, pp. 4214-4220.

[Gu 2009] Gu, D., Shen, Y. Balling phenomena in direct laser sintering of stainless steel powder: Metallurgical

mechanisms and control methods. Materials & Design, 2009, Vol. 30, No. 8, pp. 2903-2910.

[Huysmans 2021] Huysmans, S., et al. Weldability study of additive manufactured 316L austenitic stainless steel components—Welding of AM with conventional 316L components. Welding in the World, 2021, Vol. 65, No. 7, pp. 1415-1427.

[Kuehn 2024] Kuehn, K., Wang, X. Effects of gas tungsten arc welding on the mechanical properties and microstructure of 316L stainless steel by powder bed fusion. International Journal of Advanced Manufacturing Technology, 2024, Vol. 132, No. 5, pp. 2563-2573.

[Mascenik 2020] Mascenik, J., Pavlenko, S. Determination of stress and deformation during laser welding of aluminium alloys with the PC support. MM Science Journal, 2020, Vol. November, pp. 4104-4107.

[Matweb 2025] Matweb. AISI Type 316L Stainless Steel [online]. 2025. Available from https://www.matweb.com/search/DataSheet.aspx?MatGUID=530144e2752b47709a58ca8fe0849969.

[Michler 2021] Michler, M., et al. Investigation of pore reduction in hybrid joints of conventionally and additively manufactured AlSi10Mg using electron beam welding. Advanced Engineering Materials, 2021, Vol. 23, No. 6, 2001325.

[Mohyla 2022] Mohyla, P., et al. Influence of heat treatment of steel AISI316L produced by the selective laser melting method on the properties of welded joint. Materials, 2022, Vol. 15, No. 5, 1690.

[Omoniyi 2022] Omoniyi, P.O., et al. Joint integrity evaluation of laser beam welded additive manufactured Ti6Al4V sheets. Scientific reports, 2022, Vol. 12, No. 1, 4062.

[Patterson 2021] Patterson, T., et al. A review of high energy density beam processes for welding and additive manufacturing applications. Welding in the World, 2021, Vol. 65, No. 7, pp. 1235-1306.

[Renishaw 2025] Renishaw. Data sheet: SS 316L-0407 powder for additive manufacturing [online]. 2025. Available from https://www.renishaw.com/resourcecentre/en/details/data-sheet-ss-316l-0407-powder-for-additive-manufacturing--90802.

[Renishaw 2025] Renishaw. Meander Stripe and Chessboard Hatching Pattern [online]. 2025. Available from https://www.renishaw.com/resourcecentre/en/details/Meander-stripe-and-chessboard-hatchings-pattern--95492?lang=en.

[Saga 2020] Saga, M., et al. Research of the Fatigue Life of Welded Joints of High Strength Steel S960 QL Created Using Laser and Electron Beams. Materials, 2020, Vol. 13, No. 11. DOI: 10.3390/ma13112539.

[Sali 2022] Sali, A., et al. Electron beam welding of rolled and laser powder bed fused Inconel 718. International Journal of Advanced Manufacturing Technology, 2022, Vol. 120, No. 7, pp. 5451-5468.

[Selmi 2023] Selmi, H., et al. Weldability of 316L parts produced by metal additive manufacturing. Journal of Manufacturing and Materials Processing, 2023, Vol. 7, No. 2, 71.

[Sen 2023] Sen, M., Kurt, M. Comparison between laser and TIG welding of electron beam melted Ti6Al4V parts. Materials Testing, 2023, Vol. 65, No. 12, pp. 1776-1785.

[Zhang 2019] Zhang, C., et al. A comparison between laser and TIG welding of selective laser melted AlSi10Mg. Optics & Laser Technology, 2019, Vol. 120, 105696.

CONTACTS:

Matus Gelatko, Eng. MSc. PhD.
Technical University of Kosice, Faculty of Manufacturing Technologies with a seat in Presov
Sturova 31, 080 01 Presov, Slovakia
e-mail: matus.gelatko@tuke.sk